Chitosan Nanoparticle Delivery of *Prunus africana* (Hook.f) Kalkman Attenuates TGF-β/SMAD3-Driven Epithelial–Mesenchymal Transition to Suppress Prostate Cancer Metastasis

Cletus Anes Ukwubile[1,*], Hassan Braimah Yesufu [2].

1 Department of Pharmacognosy, Faculty of Pharmacy, University of Maiduguri, Maiduguri P.M.B. 1069, Borno State, Nigeria

2 Department of Pharmaceutical Chemistry, Faculty of Pharmacy, University of Maiduguri, Maiduguri P.M.B. 1069, Borno State, Nigeria

ORCID IDs
Cletus Anes Ukwubile: https://orcid.org/0000-0001-7183-4510
Hassan Braimah Yesufu: https://orcid.org/0000-0003-4351-7707

Abstract

Background: As is well known, one of the major drivers of metastatic prostate cancer is the epithelial-mesenchymal transition (EMT), which is tightly controlled by TGF-β/SMAD3 signaling. Therefore, although *Prunus africana*, which contains active phytochemicals with anticancer potential, is a drug candidate with poor solubility and limited bioavailability, these limitations may hamper its efficacy in clinical use. **Aim:** In this study, the team assessed whether vending the extract, *P. africana*, with chitosan nanoparticle delivery created a hindrance to TGF-β/SMAD3-mediated EMT and metastasis in prostate cancer cells. **Methods:** *P. africana*-loaded chitosan nanoparticles were prepared by ionic gelation with sodium tripolyphosphate and were characterized for the particle size, polydispersity index, zeta potential, encapsulation efficiency, morphology, and release profile. Antimetastatic effects were analyzed using prostate cancer cells' viability, wound-healing, transwell migration/invasion, qRT-PCR, western blotting, and immunofluorescence. TGF-β-induced EMT was established at 10 ng/mL of recombinant TGF-β1. The *in vivo* metastasis model was used to confirm the metastatic burden and pathway modulation. **Results:** Average physical properties were as follows: average diameter, 168.4 ± 12.6 nm; polydispersity index, 0.23 ± 0.04; zeta potential, +31.7 ± 3.2 mV; and entrapment efficiency, 82.6 ± 4.8%. Release from the nanoparticles reached 71.3% in 72 hours. *P. africana*-loaded chitosan nanoparticles significantly inhibited TGF-β1-induced cell migration by 64.8% and cell invasion by 69.2% relative to the TGF-β1-treated group ($p < 0.05$). It also reduced the number of lung metastases by 58.7% compared with the metastatic control group ($n = 6$ animals per group, $p <$

0.05). This treatment downregulated TGF-β-induced SMAD3 phosphorylation, followed by downregulation of N-cadherin and vimentin, Snail, Slug, and Twist, and restoration of E-cadherin. *In vivo* studies demonstrated a significant reduction in metastatic sites (58.7%) and pSMAD3 expression with nanoparticles. **Conclusion:** Chitosan nanoparticle intervention enforced an antimetastatic effect of *P. africana* by dimming off TGF-β/SMAD3-mediated EMT, suggesting this as a potential nanophytotherapeutic against prostate cancer metastases.

Keywords: *Prunus africana*; chitosan nanoparticles; prostate cancer; TGF-β/SMAD3; epithelial–mesenchymal transition.

1. Introduction

Prostate cancer is one of the most frequently diagnosed malignancies among men throughout the world, and metastatic progression remains the major determinant of a poor clinical outcome[1]. Often, localized prostate cancer can be treated effectively using curative-intended therapeutic measures such as surgery, radiation therapy, androgen-deprivation therapy, and other systemic paradigms, but the advanced disease becomes invasive, resistant to therapy, and tends to spread[2]. In particular, these spread elements end up in bone and lymphatic tissues. The biological conversion of localized tumor growth to metastatic disease involves the coordinated remodeling of cell adhesion, cytoskeletal organization, ECM interactions, immune escape, and survival under anchorage-independent conditions[1,3].

Epithelial–mesenchymal transition (EMT) is the most important thing that speeds up cancer[4,5]. In that procedure, cancerous epithelial cells lose their polarity, cell adhesion, and gain traits prevailing for moving, invading, and also stemness and apoptosis prevention. In prostate cancer, EMT is linked to disease aggressiveness, onset of metastasis, resistance to therapy, and poor prognosis. These transformations are hallmarked by loss of epithelial markers such as E-cadherin and gain of mesenchymal markers such as N-cadherin and vimentin, as well as factors such as Snail, Slug, Twist, and metalloproteinases [6].

One of the major causative pathways of EMT in cancer progression is the signaling of the transforming growth factor β [7,8]. For lethally transformed prostate epithelium, β-transforming growth factor possesses tumor suppressor activities through the inhibition of cell proliferation and stimulation of apoptosis. However, in the advanced prostate tumors, tumor cells become resistant to TGFβ-induced growth inhibition while maintaining the proinvasive, prometastatic activities of

TGFβ [8,9]. This context-dependent switch enables TGFβ to promote epithelial-mesenchymal transition, migration, invasion, immune evasion, and metastatic colonization. SMAD3 is a critical downstream mediator of canonical TGF-β signaling, which is prominently involved in transcriptional regulation of the genes associated with the EMT [10,11].

Natural products are one of the most important sources of anticancer agents because their bioactive constituents function by interfering with multiple pathways of cancerogenic transformation [12,13]. Originating from African traditional medicine, *Prunus africana* is a widely used medicinal plant for prostate-related conditions. According to earlier reviews, *P. africana* is rich in phytochemicals like sterols, triterpenoids, phenolic compounds, and fatty acids; moreover, its reported capacities include processes of antiandrogenic, antiangiogenic, antiproliferative, and pro-apoptotic properties in prostate cancer models [14–16]. However, like many plant-derived extracts, its therapeutic potential is compromised by the limited aqueous solubility, variable stability, low bioavailability, and non-selective distribution in tissues.

Nanoparticle-based drug delivery is an encouraging strategy to enhance the therapeutic performance of phytochemicals. Chitosan, which is a biodegradable, biocompatible, cationic polysaccharide, has seen applications for drug and phytochemical delivery. Ionic gelation with sodium tripolyphosphate can be used for the synthesis of chitosan nanoparticles, a very straightforward process, avoiding the use of harsh organic solvents and providing nanoscale encapsulation of bioactive compounds. While nanoscale encapsulation improves solubility, cellular uptake, biotransformation shielding, and sustained release, such chitosan-based nanoparticles have shown a great deal of focus as they introduce a new dimension of exploring nanoparticles for drug delivery [17–19].

Though traditionally used for medicinal purposes, *P. africana* has never been fully explored to understand the possible role of chitosan nanoparticle formulation in interfering with the antimetastatic effects of *P. africana* in prostate cancer through modulation of TGF-β/SMAD3-involved EMT. This work was, therefore, aimed at preparing and characterizing chitosan nanoparticles formulated with *P. africana* for their effect on the inhibition of migration and invasion of prostate cancer, EMT, and abrogation of metastasis *in vivo*. We speculate that with the chitosan nanocarrier, the bioactives of *P. africana* shall be more available intracellularly and would

hinder the TGF-β1/SMAD3 signaling pathway responsible for EMT and thereby inhibit metastasis.

2. Materials and Methods

2.1. Materials, Chemicals, and Apparatus

Low-molecular-weight chitosan (deacetylation degree ≥ 85%) and sodium tripolyphosphate (TPP) were purchased from Sigma–Aldrich (St. Louis, MO, USA). Methanol (HPLC grade), acetonitrile (LC–MS grade), formic acid, gallic acid, quercetin, Folin–Ciocalteu reagent, aluminium chloride, dimethyl sulfoxide (DMSO), phosphate-buffered saline (PBS), and other analytical-grade reagents were obtained from Merck KGaA (Darmstadt, Germany) unless otherwise stated. Ultrapure water was generated using a Milli-Q water purification system (Millipore, Bedford, MA, USA). Cell culture reagents, including Dulbecco's Modified Eagle Medium (DMEM), fetal bovine serum (FBS), penicillin–streptomycin solution, trypsin–EDTA, and phosphate-buffered saline, were obtained from Gibco (Thermo Fisher Scientific, Waltham, MA, USA). Recombinant human transforming growth factor-beta 1 (TGF-β1) was purchased from PeproTech (Rocky Hill, NJ, USA). Particle size, polydispersity index, and zeta potential measurements were performed using a Zetasizer Nano ZS (Malvern Panalytical, Worcestershire, UK). Morphological characterization was carried out using a scanning electron microscope (SEM; JSM-IT200, JEOL Ltd., Tokyo, Japan). UV–Visible spectrophotometric measurements were performed using a UV-1800 spectrophotometer (Shimadzu Corporation, Kyoto, Japan). Freeze-drying was conducted using a Labconco FreeZone lyophilizer (Labconco Corporation, Kansas City, MO, USA), while solvent removal was achieved using a rotary evaporator (Buchi R-300, Büchi Labortechnik AG, Flawil, Switzerland).

2.2. Plant Collection, Authentication, and Extraction

Fresh stem bark of *Prunus africana* was collected in 2026 during the morning hours (6:00–7:00 a.m.) from a forested area in Plateau State, Nigeria. The plant material was authenticated by Dr. C. A. Ukwubile, Department of Pharmacognosy, University of Maiduguri, Nigeria. A voucher specimen (UMM/FPH/ROA/001) was deposited in the departmental herbarium for future reference. The collected stem bark was washed with distilled water to remove adhering debris, shade-dried at ambient temperature (25–28°C) for 21 days, and pulverized using a laboratory grinder. The powdered material was extracted with 70% methanol (1:10 w/v) by cold maceration for 48 h with intermittent agitation. The extract was filtered through Whatman No. 1 filter paper and concentrated under reduced pressure using a rotary evaporator at 40°C. The concentrated extract was subsequently freeze-dried and stored at −20°C until further use.

2.3. Phytochemical Standardization

2.3.1. Phytochemical Analysis

Each extract batch was subjected to phytochemical standardization before nanoparticle formulation. Total phenolic content (TPC) was determined using the Folin–Ciocalteu method and expressed as mg gallic acid equivalent (GAE)/g extract, while total flavonoid content (TFC) was determined by the aluminium chloride colorimetric method and expressed as mg quercetin equivalent (QE)/g extract.

2.3.2. LC–MS Analysis

LC–MS analysis was performed using a high-performance liquid chromatography system coupled to a quadrupole time-of-flight mass spectrometer (LC–QTOF–MS) equipped with an electrospray ionization (ESI) source. Chromatographic separation was achieved on a C18 reversed-phase column (150 × 2.1 mm, 1.7 μm particle size) maintained at 40°C. The mobile phase consisted of solvent A (0.1% formic acid in water) and solvent B (acetonitrile containing 0.1% formic acid). Elution was carried out using a gradient program of 5–95% solvent B over 30 min at a flow rate of 0.30 mL/min. The injection volume was 5 μL. Mass spectrometric detection was performed in both positive and negative ionization modes under the following conditions: capillary voltage, 3.5 kV; source temperature, 120°C; desolvation temperature, 350°C; desolvation gas (nitrogen) flow rate, 800 L/h; cone gas flow rate, 50 L/h; nebulizer pressure, 35 psi; and collision energy, 10–40 eV. Data were acquired over a mass scan range of *m/z* 100–1500. Mass calibration was performed using a standard calibration solution before analysis. Identification of phytochemical constituents was achieved by comparing retention times, accurate masses, and fragmentation patterns with those of authentic reference standards and published databases.

2.3.3. Quantification of Marker Compounds

Quantification of β-sitosterol, ursolic acid, oleanolic acid, and ferulic acid was performed using external calibration curves generated from authenticated reference standards. Calibration curves exhibited good linearity ($R^2 > 0.995$) over the concentration ranges evaluated. All analyses were performed in triplicate.

2.3.4. Batch-to-Batch Repeatability

Three independent extract batches were analyzed under identical conditions. The relative standard deviation (RSD) values for retention times and peak areas of the principal marker compounds were less than 5%, confirming acceptable batch-to-batch reproducibility.

2.3.5. Microbial Quality

Microbial quality assessment was conducted according to the requirements of the current pharmacopoeial guidelines, including the European Pharmacopoeia and United States Pharmacopeia (USP <61> and USP <62>). Total aerobic microbial count, total yeast and mould count, and the absence of specified pathogenic microorganisms were confirmed to be within acceptable limits.

2.3.6. Heavy Metal Analysis

Heavy metal analysis was performed in accordance with the limits established by the World Health Organization (WHO) and relevant pharmacopoeial standards. Levels of lead (Pb), cadmium (Cd), arsenic (As), and mercury (Hg) were below the permissible limits for herbal medicinal materials.

Only extract batches that demonstrated consistent phytochemical profiles, acceptable batch-to-batch reproducibility, and compliance with microbial and heavy-metal specifications were selected for nanoparticle preparation [20,21].

2.4. Preparation of *Prunus africana*-Loaded Chitosan Nanoparticles

Prunus africana-loaded chitosan nanoparticles were prepared by the ionic gelation method using chitosan and sodium tripolyphosphate (TPP) as the polymer and cross-linking agent, respectively. Low-molecular-weight chitosan was dissolved in 1% (v/v) acetic acid to obtain a 0.25% (w/v) chitosan solution. The pH of the solution was adjusted to 5.5 using 0.1 M sodium hydroxide and stirred overnight to ensure complete polymer hydration. For the optimized formulation (F5), 50 mg of freeze-dried *P. africana* extract was dispersed in 20 mL of the chitosan solution and stirred magnetically at 1000 rpm for 30 min at room temperature (25 ± 2°C) to obtain a homogeneous dispersion. Separately, a 0.10% (w/v) TPP solution was prepared in distilled water and filtered

through a 0.45 μm membrane filter before use. Nanoparticles were formed by adding the TPP solution dropwise to the chitosan–extract dispersion at a chitosan: TPP mass ratio of 2.5:1. The TPP solution was added at a controlled rate of approximately 1 mL/min under continuous magnetic stirring at 1000 rpm. Following complete addition of the cross-linking solution, the reaction mixture was further stirred for 30 min at room temperature to allow complete ionic gelation and nanoparticle stabilization. The resulting nanoparticle suspension was centrifuged at 15,000 rpm for 30 min at 4°C. The pellet was washed three times with distilled water to remove unentrapped extract and excess TPP, followed by recentrifugation under the same conditions after each washing step. The purified nanoparticles were frozen at −80°C and subsequently lyophilized using a freeze dryer for 48 h to obtain a dry nanoparticle powder. The lyophilized nanoparticles were stored in airtight containers at 4°C until further characterization and biological evaluation. Blank chitosan nanoparticles were prepared using the same procedure but without the addition of *P. africana* extract [17,19].

2.5. Nanoparticle Characterization

Mean particle size, polydispersity index, and zeta potential were acquired by dynamic light scattering. The morphology was observed by scanning electron microscopy. Encapsulation efficiency and loading capacity were determined after separation of free plant extract from the nanoparticles using the process of centrifugation.

Encapsulation efficiency was calculated as:

$$\text{Encapsulation efficiency (\%)} = [\text{Total extract added} - \text{Free extract in supernatant}) / \text{Total extract added}] \times 100 \quad (1)$$

Loading capacity was calculated as:

$$\text{Loading capacity (\%)} = [(\text{Total extract encapsulated}) / \text{Weight of nanoparticles}] \times 100 \quad (2)$$

The release *in vitro* was evaluated by suspending the nanoparticles in Phosphate Buffer Saline at pH 7.4 or buffer at pH 5.5 to imitate physiological and lower acidic tumor/endosomal conditions. At every specific moment, samples were collected, centrifuged, and examined for the liberated plant content [19].

2.5.1. Release Kinetic Modeling

To elucidate the release mechanism of *P. africana*-loaded chitosan nanoparticles, the cumulative *in vitro* release data obtained at pH 5.5 and pH 7.4 were fitted to various mathematical kinetic models, including Zero-order, First-order, Higuchi, and Korsmeyer–Peppas models. The release data were analyzed using nonlinear regression analysis in GraphPad Prism version 9 (GraphPad Software, San Diego, CA, USA).

2.6. Cell Culture

Human prostate cancer cell lines LNCaP, along with the normal prostate epithelial cells RWPE-1, were procured from the American Type Culture Collection (ATCC). The cells were propagated in RPMI and DMEM media with 10% fetal bovine serum and 1% penicillin-streptomycin at 37°C under a humid condition of 5% CO_2.

2.7. Experimental Treatment Groups

Cells were accordingly grouped: normal with no treatment, usages of blank chitosan nanoparticles, use of free *P. africana* extract, fulfills of *P. africana* into chitosan nanoparticles, TGF-β alone, TGF-β along with free *P. africana* extract, TGF-β and *P. africana*-loaded chitosan nanoparticles, and TGF-β and SMAD3 inhibitor or siSMAD3 as the mechanistic control dots of the thing. Free *P. africana* extract was at extract-equivalent concentrations of 25, 50, and 100 µg/mL, while chitosan nanoparticles were at the corresponding nanoparticle-mass equivalents. Cells were treated with recombinant human TGF-β1 at 10 ng/mL for 24–48 h to allow epithelial–mesenchymal transition modifications. During mechanistic validation, some cells were treated with the SMAD3 inhibitor SIS3 at 5 µM or transfected with 20–50 µM siSMAD3 before TGF-β1 stimulation. Subsets of these assays assessed viability after 24, 48, and 72 hours, migration, and invasion responded accordingly within 24-and 48 h of incubation, whereas qRT-PCR, Western blot analysis, and immunofluorescence staining after 24–48 h of treatment [22,23].

2.8. Cell Viability and Selectivity Assay

The cytotoxic effects of *P. africana* extract, blank chitosan nanoparticles, and *P. africana*-loaded chitosan nanoparticles were evaluated using the MTT cell viability assay. Human prostate cancer cells and normal prostate epithelial cells were seeded into 96-well plates at a density of 5×10^3

cells per well in 100 µL of complete culture medium and allowed to attach for 24 h under standard culture conditions (37°C, 5% CO_2, and 95% relative humidity). Following attachment, cells were treated with various concentrations of the test samples (0–200 µg/mL) and incubated for 72 h. Untreated cells served as the negative control, while medium without cells served as the blank control. After treatment, 20 µL of MTT solution (5 mg/mL in phosphate-buffered saline) was added to each well, and the plates were incubated for an additional 4 h at 37°C. The culture medium was then carefully removed, and the resulting formazan crystals were dissolved in 150 µL of dimethyl sulfoxide (DMSO). Absorbance was measured at 570 nm using a microplate reader.

Cell viability was calculated according to the following equation:

$$\text{Cell Viability (\%)} = \frac{\text{Absorbance of treated cells}}{\text{Absorbance of control cells}} x\ 100 \quad (1)$$

Dose–response curves were generated using nonlinear regression analysis in GraphPad Prism version 9 (GraphPad Software, San Diego, CA, USA), and the half-maximal inhibitory concentration (IC_{50}) values were determined for each treatment.

The selectivity index (SI) was calculated to evaluate the preferential cytotoxicity of the formulations toward prostate cancer cells relative to normal prostate epithelial cells using the following equation:

$$SI = \frac{IC_{50}\ (\text{RWPE\_1 normal prostate epithelial cells})}{IC_{50}\ (\text{LNCaP prostate cancer cells})} \quad (2)$$

An SI value greater than 2 was considered indicative of selective anticancer activity. All experiments were performed in triplicate and repeated at least three times independently[24–26].

2.9. Cellular Uptake Study

Fluorescein isothiocyanate (FITC) dye-labeled nanoparticles were incubated with prostate cancer cells that took up these nanoparticles in 24 hours. These cells were observed under fluorescence microscopy and flow cytometry to observe for accumulated FITC signals. The intracellular localization techniques were applied in the presence of organelle markers, including lysosomal or endosomal markers [26,27].

2.10. Wound-Healing Migration Assay

Cells were seeded in six-well plates and allowed to grow to approximately 90%-100% confluence. A uniform linear scratch was created where each monolayer was subjected to damaged tissue using a sterile 200 µL pipette tip, followed by the clearing of the floating cells by washing twice with phosphate-buffered saline. Cells were cultured in serum-reduced medium containing 1% fetal bovine serum for the relevant experimental groups. Images of the wound area were taken at 0, 12, and 24 h using an inverted microscope. The percentage of wound closure was calculated by ImageJ software and was done relative to the initial wound width at 0 h [28,29].

2.11. Transwell Migration and Matrigel Invasion Assays

In the migration assay, the cultured cells were serum-starved, detached, and seeded in serum-free medium in the upper chambers of Transwell inserts. The lower chambers contained medium with 10% FBS as the chemoattractant. This assay was carried out for 24 hours, at the end of which any non-migrated cells on the upper side of the membrane were gently wiped out. Migrated cells on the lower surface of the membrane were then fixed for 15 min with 4% formaldehyde and stained for 20 min with 0.1% crystal violet. For the invasion assay, transwell inserts were layered with Matrigel after polymerizing for 1 h at 37 °C before the addition of cells. Cells that invaded were counted after 48 h, fixed and stained, and counted in at least five randomly selected microscopic fields per insert. Migration and invasion rates were expressed as percentages relative to the untreated control [30].

2.12. Quantitative Real-Time Polymerase Chain Reaction

Total RNA was isolated from treated prostate cells through TRIzol™ extraction according to the manufacturer's protocol. RNA quantitation and purity were spectroscopically analyzed, followed by cDNA synthesis using a transcription kit. The RT-PCR method employing SYBR Green qPCR Master Mix was done on a real-time PCR system to measure the expression levels of CDH1, CDH2, VIM, SNAI1, SNAI2, TWIST1, MMP2, MMP9, TGFB1, SMAD3, and relevant markers related to epithelial-mesenchymal transition. The gene expression was normalized to GAPDH as an internal control gene, and the relative fold change compared to the control sample was calculated using the 2ˆ-ΔΔCt method [25,27,31].

2.13. Western Blotting

The total protein was extracted, quantified, separated by SDS-PAGE, and transferred onto membranes made up of polyvinylidene difluoride. Those membranes were incubated with various primary antibodies, including E-cadherin, N-cadherin, vimentin, Snail, Slug, Twist, TGF-β receptor I, total SMAD3, phosphorylated SMAD3, and β-actin. The chemiluminescent bands with proteins were visualized; the density was determined by densitometry[22,29].

2.14. Immunofluorescence Staining

Cells under treatment were fixed, permeabilized, blocked, and then incubated with antibodies against E-cadherin, vimentin, and phospho-SMAD3. Nuclei were counterstained with DAPI. Acquired images were obtained by turning on fluorescence on confocal microscopy[32,33].

2.15. *In Vivo* Metastasis Study

Eight-week-old male athymic nude mice (20–25 g) were obtained from the institutional animal facility and maintained under standard laboratory conditions (22 ± 2°C, 55 ± 10% relative humidity, and a 12 h light/dark cycle) with free access to food and water. All animal procedures were conducted in accordance with the guidelines for the care and use of laboratory animals and were approved by the Institutional Animal Ethics Committee (Approval No. FP/03/24/SP.9788). Experimental metastasis was established by intravenous injection of luciferase-expressing prostate cancer cells via the tail vein of the animals. Following tumor-cell inoculation, the animals were randomly assigned to five groups (n = 6 mice per group) as follows:

- *Group I (normal control*): Healthy mice receiving vehicle only (0.9% saline, 10 mL/kg, oral gavage), without tumor-cell inoculation.
- *Group II (metastatic control):* Tumor-bearing mice receiving vehicle only (0.9% saline, 10 mL/kg, oral gavage).
- *Group III (blank chitosan nanoparticles):* Tumor-bearing mice treated with blank chitosan nanoparticles at a dose equivalent to the nanoparticle carrier used in Group V (200 mg/kg, oral gavage).
- *Group IV (free P. africana extract):* Tumor-bearing mice treated with free *P. africana* extract (100 mg/kg body weight, oral gavage).

- *Group V (P. africana-loaded chitosan nanoparticles):* Tumor-bearing mice treated with *P. africana*-loaded chitosan nanoparticles containing an equivalent *P. africana* extract dose of 200 mg/kg body weight (oral gavage).

Treatments were administered three times per week for six consecutive weeks. Body weight, clinical signs, tumor progression, and metastatic dissemination were monitored throughout the study. Treatments were administered according to the predetermined dosing schedule throughout the experimental period. Tumor progression and metastatic dissemination were monitored using in vivo bioluminescence imaging and micro-computed tomography (micro-CT). At the end of the study, animals were euthanized, and major organs, including the lungs, liver, and tumor-bearing tissues, were collected for further analyses.

Metastatic burden was assessed by gross examination, histopathological evaluation, and tissue-specific tumor-marker analysis. In addition, immunohistochemical and molecular analyses were performed to evaluate the expression of epithelial–mesenchymal transition (EMT)-related proteins and components of the TGF-β/SMAD3 signaling pathway. The extent of metastatic lesions and treatment-associated histological changes was quantified and compared among the experimental groups [34–36].

2.16. Statistical Analysis

Data were expressed as mean ± SD (n = 3). Statistical comparisons were performed using one-way analysis of variance followed by Tukey's post hoc test or two-way analysis of variance where appropriate. Survival or metastasis-free outcomes were analyzed using Kaplan–Meier curves and the log-rank test. Statistical significance was computed at a p-value < 0.05.

3. Results

3.1. Phytochemical contents

During the phytochemical screening studies on the extract, diverse large preparations of *P. africana* extracts show remarkably repeatable chemical profiles, with several chemical constituents clearly present, like β-sitosterol, ursolic acid, oleanolic acid, ferulic acid, stigmasterol, and campesterol, which act as main lead compounds. Both phytochemical extracts also have

noticeable total phenolic and flavonoid amounts, and this points to possible antioxidant as well as bioactive functions. In microbial screening, *E. coli* and *Salmonella* spp. were not detected, so total aerobic microbial, yeast, and mould counts were kept close to the preset thresholds. On further consideration, the outcomes brought output data in congruence with the selected batch, which did exude some heavy metals, actually low levels of lead, cadmium, arsenic, and mercury. It serves as an indicator of sufficiency in later nanoparticles and biological evaluation selection (Table 1).

Table 1: Phytochemical content and quality fingerprints of *P. africana* nanoformulation

Parameter	Method	Result	Unit	Interpretation
Total phenolic content	Folin–Ciocalteu assay	128.64 ± 4.72	mg gallic acid equivalent/g extract	High phenolic content
Total flavonoid content	Aluminum chloride colorimetric assay	76.38 ± 3.15	mg quercetin equivalent/g extract	Appreciable flavonoid content
β-Sitosterol	LC–MS	18.42 ± 0.86	mg/g extract	Major phytosterol marker detected
Ursolic acid	LC–MS	11.76 ± 0.54	mg/g extract	Major triterpenoid marker detected
Oleanolic acid	LC–MS	9.84 ± 0.41	mg/g extract	Triterpenoid marker detected
Ferulic acid	LC–MS	4.28 ± 0.19	mg/g extract	Phenolic acid marker detected
Campesterol	LC–MS	3.62 ± 0.22	mg/g extract	Minor phytosterol detected
Stigmasterol	LC–MS	5.47 ± 0.31	mg/g extract	Phytosterol marker detected
Total aerobic microbial count	Plate count method	1.8×10^2	CFU/g	Within an acceptable limit
Total yeast and mould count	Plate count method	$<1.0 \times 10^1$	CFU/g	Within an acceptable limit
Escherichia coli	Culture method	Not detected	CFU/g	Acceptable
Salmonella spp.	Culture method	Not detected	CFU/25 g	Acceptable
Lead	AAS/ICP–MS	0.42 ± 0.03	mg/kg	Within an acceptable limit
Cadmium	AAS/ICP–MS	0.06 ± 0.01	mg/kg	Within an acceptable limit
Arsenic	AAS/ICP–MS	0.09 ± 0.01	mg/kg	Within an acceptable limit
Mercury	AAS/ICP–MS	0.02 ± 0.01	mg/kg	Within an acceptable limit

Data are presented as mean ± SD (n = 3).

3.2. Characterization of nanoparticles

Table 2 displays the composition and optimization profile of the chitosan nanoparticles loaded with Prunus africana, and Figure 1 displays the physicochemical characterization of the optimized

formulation. Particle size, polydispersity index, zeta potential, encapsulation efficiency, and loading capacity were significantly impacted by differences in chitosan concentration, TPP concentration, chitosan: TPP ratio, and extract loading across the formulation batches. Higher concentrations enhanced loading capacity but also encouraged particle enlargement and decreased size uniformity, while formulations with lower polymer and crosslinker concentrations generated smaller nanoparticles but demonstrated relatively poorer extract encapsulation.

Because formulation F5 offered the best balance between particle size, homogeneity, surface charge, encapsulation efficiency, and loading capacity among the prepared batches, it was chosen as the optimized nanoparticle formulation. F5 had 50 mg of *P. africana* extract, 0.25% w/v chitosan, 0.10% w/v TPP, and a chitosan: TPP ratio of 2.5:1. With a mean particle size of 168.4 ± 12.6 nm, a polydispersity index of 0.23 ± 0.04, and a zeta potential of +31.7 ± 3.2 mV, this formulation yielded nanoparticles. A narrow and homogeneous particle-size distribution is indicated by the comparatively low polydispersity index, and strong colloidal stability is suggested by the positive zeta potential, which represents the cationic character of chitosan. Additionally, by facilitating contact with negatively charged cancer cell membranes, this positive surface charge may enhance cellular absorption. With an encapsulation efficiency of 82.6 ± 4.8% and a loading capacity of 21.4 ± 1.6%, the improved formulation further showed significant extract incorporation. Formulations F6–F8 produced larger particles with greater polydispersity values, indicating increased aggregation propensity and decreased appropriateness for biological evaluation, albeit having a somewhat higher loading capacity. As a result, F5 was thought to be the best formulation for further *in vitro* and *in vivo* research. The optimized nanoparticles had a significant positive surface charge and a restricted nanoscale size distribution, as seen in Figure 1A and B.

Morphological checking using SEM showed mostly circular, distinct, smooth-surfaced particles, though there was limited aggregation (Figure 1C). The nano-encapsulated extract entrapped more drug (Figure 1D). *In vitro* release displayed a sustained and pH- responsive release behavior across 72 h, and it looked pretty consistent. At physiological pH 7.4, the total extract release reached 71.3 ± 5.5%. Meanwhile, at a more acidic pH of 5.5, release went up to 86.4 ± 5.8 (Figure 1E). That larger release under acidic settings implies the nanoparticles may favor expelling the *P. africana* bioactives inside acidic tumor zones or within endosomal compartments.

To elucidate the release mechanism of the optimized Prunus africana-loaded chitosan nanoparticles (F5), the in vitro release data obtained at pH 5.5 and pH 7.4 were fitted to Zero-order, First-order, Higuchi, and Korsmeyer–Peppas kinetic models (Table 3). Among the models evaluated, the Korsmeyer–Peppas model exhibited the highest correlation coefficients ($R^2 = 0.989$ at pH 5.5 and 0.981 at pH 7.4), indicating that it best described the release behavior of the nanoparticles. The release exponent values (n = 0.63 at pH 5.5 and n = 0.58 at pH 7.4) suggested a non-Fickian or anomalous transport mechanism, whereby drug release was controlled by both diffusion through the polymer matrix and polymer relaxation/erosion processes. The higher release rate constant observed under acidic conditions further supports the pH-responsive nature of the chitosan nanoparticles, which may facilitate enhanced release of bioactive constituents within acidic tumor microenvironments and intracellular endosomal compartments (Table 3). Taken together, the optimization and characterization results indicate that F5 had workable nanoscale properties, strong extract encapsulation, acceptable loading, reliable colloidal stability, and continued pH-sensitive release, which then supports choosing it for the later antimetastatic assays.

Table 2: Formulations of *P. africana*-loaded chitosan nanoparticles: composition and optimization

Formulation code	Chitosan (% w/v)	TPP (% w/v)	Chitosan: TPP ratio	*P. africana* extract (mg)	Particle size (nm)	PDI	Zeta potential (mV)	Encapsulation efficiency (%)	Loading capacity (%)	Remarks
F1	0.10	0.05	2:1	25	142.6 ± 8.4	0.31 ± 0.03	+24.8 ± 2.1	68.4 ± 3.7	12.6 ± 0.9	Small size but moderate loading
F2	0.15	0.05	3:1	25	158.2 ± 10.1	0.27 ± 0.02	+28.6 ± 2.4	74.9 ± 4.1	14.8 ± 1.1	Improved stability and loading
F3	0.20	0.05	4:1	25	181.7 ± 11.5	0.24 ± 0.03	+31.2 ± 2.7	79.5 ± 4.3	16.9 ± 1.2	Good particle uniformity
F4	0.20	0.10	2:1	50	214.3 ± 13.8	0.29 ± 0.04	+26.4 ± 2.3	77.8 ± 3.9	18.7 ± 1.4	Larger particles formed

Formulation code	Chitosan (% w/v)	TPP (% w/v)	Chitosan: TPP ratio	*P. africana* extract (mg)	Particle size (nm)	PDI	Zeta potential (mV)	Encapsulation efficiency (%)	Loading capacity (%)	Remarks
F5	0.25	0.10	2.5:1	50	168.4 ± 12.6	0.23 ± 0.04	+31.7 ± 3.2	82.6 ± 4.8	21.4 ± 1.6	Optimized formulation
F6	0.30	0.10	3:1	50	236.8 ± 15.4	0.34 ± 0.05	+34.5 ± 3.5	84.1 ± 5.2	22.1 ± 1.8	High loading but reduced uniformity
F7	0.25	0.15	1.7:1	75	289.5 ± 18.7	0.41 ± 0.06	+21.9 ± 2.8	80.7 ± 4.6	24.3 ± 2.0	Aggregation tendency
F8	0.30	0.15	2:1	75	315.2 ± 21.3	0.46 ± 0.07	+19.6 ± 2.5	83.5 ± 5.0	25.8 ± 2.3	Large particles; less suitable

TPP stands for sodium tripolyphosphate, and PDI for polydispersity index. The values are reported as mean ± SD of triplicate measurements.

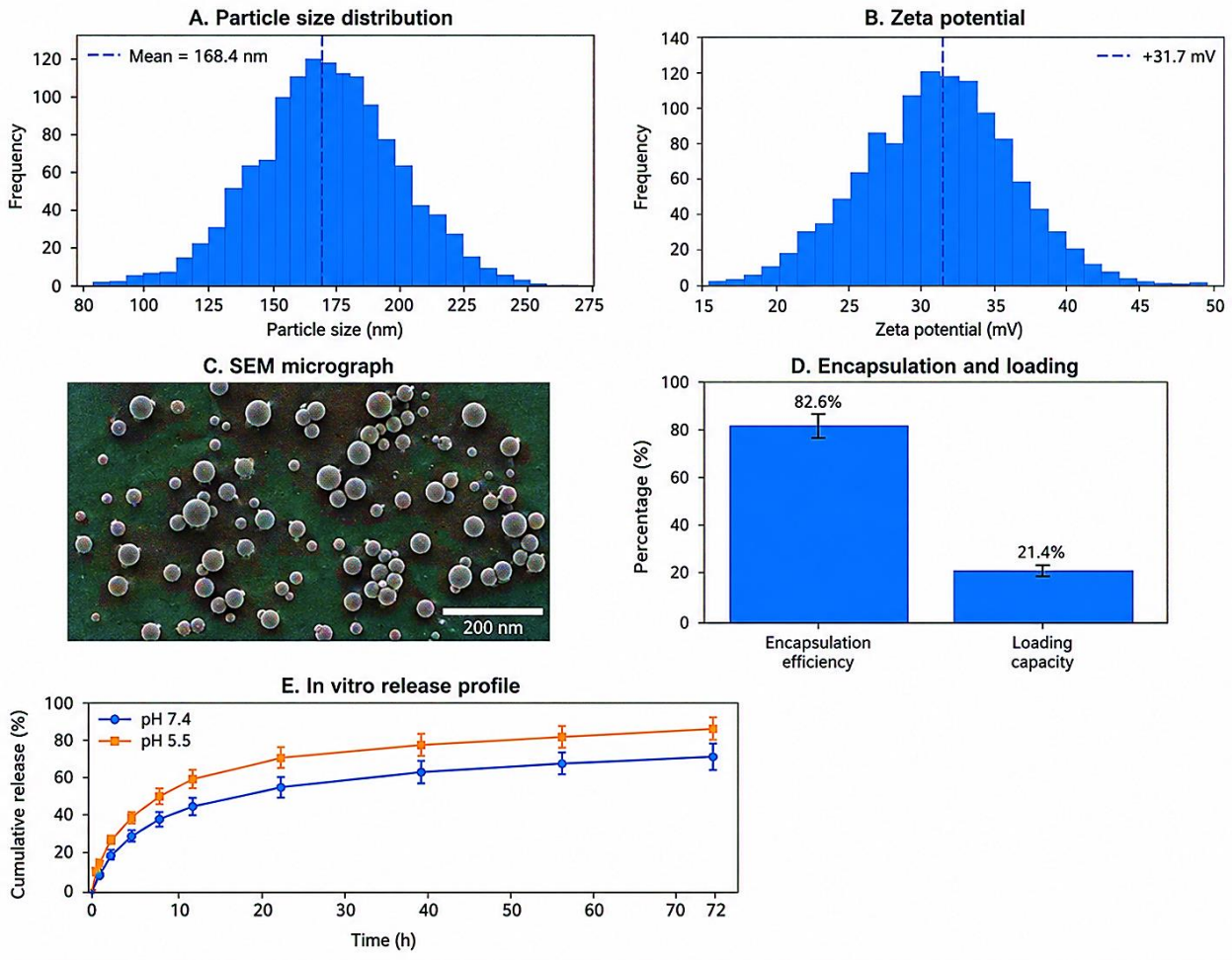

Figure 1: Optimized chitosan nanoparticles loaded with *Prunus africana* are characterized physicochemically. A: Dynamic light scattering investigation reveals a mean particle size of 168.4 ± 12.6 nm and a PDI of 0.23 ± 0.04. B: The zeta potential analysis reveals a +31.7 ± 3.2 mV positive surface charge. C: SEM micrograph of discrete, smooth-surfaced, spherical nanoparticles with little aggregation. D: The improved formulation's loading capacity and encapsulation efficiency were found to be 21.4 ± 1.6% and 82.6 ± 4.8%, respectively. E: *Prunus africana* extract was released steadily over 72 hours in vitro, with a quicker release at pH 5.5 than at pH 7.4. The mean ± SD of triplicate determinations is used to express the values.

Table 3: Kinetic modeling of in vitro release of *P. africana*-loaded chitosan nanoparticles (F5) at pH 5.5 and pH 7.4

Kinetic model	Parameter	pH 5.5	pH 7.4
Zero-order	k_0 (% h^{-1})	1.18	0.98
	R^2	0.921	0.908
First-order	k_1 (h^{-1})	0.038	0.029
	R^2	0.948	0.936
Higuchi	kH (% $h^{-1/2}$)	10.84	8.96

Kinetic model	Parameter	pH 5.5	pH 7.4
Korsmeyer–Peppas	R^2	0.972	0.964
	kKP	0.284	0.241
	n	0.63	0.58
	R^2	0.989	0.981
	Release mechanism	Non-Fickian (anomalous) transport	Non-Fickian (anomalous) transport

Values represent kinetic parameters obtained by fitting cumulative release data to Zero-order, First-order, Higuchi, and Korsmeyer–Peppas models. The Korsmeyer–Peppas model showed the highest coefficient of determination (R^2) at both pH conditions, indicating the best fit to the experimental release data. The release exponent (n = 0.58–0.63) suggests anomalous (non-Fickian) transport, implying that a combination of diffusion and polymer relaxation/erosion mechanisms governed the release of phytoconstituents from the chitosan matrix.

3.3. Cell viability and uptake assay

The study examined the cytotoxic effects and cellular absorption functions of *Prunus africana*-loaded chitosan nanoparticles in LNCaP prostate cancer cells and RWPE-1 normal prostate epithelial cells. Both free *P. africana* extract and *P. africana*-loaded chitosan nanoparticles reduced LNCaP cell survival through concentration- and time-dependent effects, as shown by the data shown in Figure 2A. The nanoparticle-loaded formulation produced stronger inhibitory effects than the free extract at matching extract concentrations. *P. africana*-loaded chitosan nanoparticles at 100 µg/mL reduced LNCaP cell viability to 42.6% after 24 h and to 25.7% after 48 h, and to 18.6% after 72 h, whereas the free extract produced 58.8% viability at 24 h and 39.8% at 48 h, and 31.2% at 72 h. RWPE-1 normal prostate epithelial cells exhibited greater treatment survival rates, which demonstrated that the treatment selectively killed prostate cancer cells. The results in Figure 2B showed that blank chitosan nanoparticles preserved RWPE-1 cell viability above 93% during all tested concentrations, which proved the relative safety of the carrier system. The free extract and nanoparticle-loaded extract demonstrated low toxicity in RWPE-1 cells because cell survival remained above 76% even at the maximum concentration studied. The IC_{50} analysis demonstrated that the nanoparticle formulation achieved higher effectiveness than previous contact. The IC_{50} values for *P. africana*-loaded chitosan nanoparticles showed lower values than free extract values at both 48 h and 72 h, according to Figure 2C. At 48 h, the IC_{50} value dropped from 63.8 µg/mL for free extract to 43.2 µg/mL for nanoparticle-loaded extract, and at 72 h it fell from 49.6 µg/mL to 31.8 µg/mL. The research demonstrates that the chitosan

nanoparticle delivery system increased *P. africana* antiproliferative effects against LNCaP prostate cancer cells.

The research found that the study resulted in better results because the researchers used nanoparticles to deliver the extract. The study showed that FITC-labelled *P. africana*-loaded chitosan nanoparticles produced a continuous increase in FITC-positive LNCaP cells, which reached 84.9% after 6 hours, while the free extract/FITC-treated cells achieved 38.6% of this result (Figure 2D-F). The study showed that the nanoparticle-treated group had higher relative fluorescence intensity at 4 hours than the free extract group because they achieved 6.9-fold results, while the free extract group achieved 2.6-fold results (Figure 2E). The fluorescence microscopy images confirmed that LNCaP cells showed higher intracellular nanoparticle fluorescence after treatment with FITC-labelled *P. africana*-loaded chitosan nanoparticles (Figure 2E-F). The study showed that chitosan nanoparticle delivery improved cell absorption of *P. africana*, which produced stronger toxic effects against prostate cancer cells but resulted in lower harmful effects on normal prostate epithelial cells.

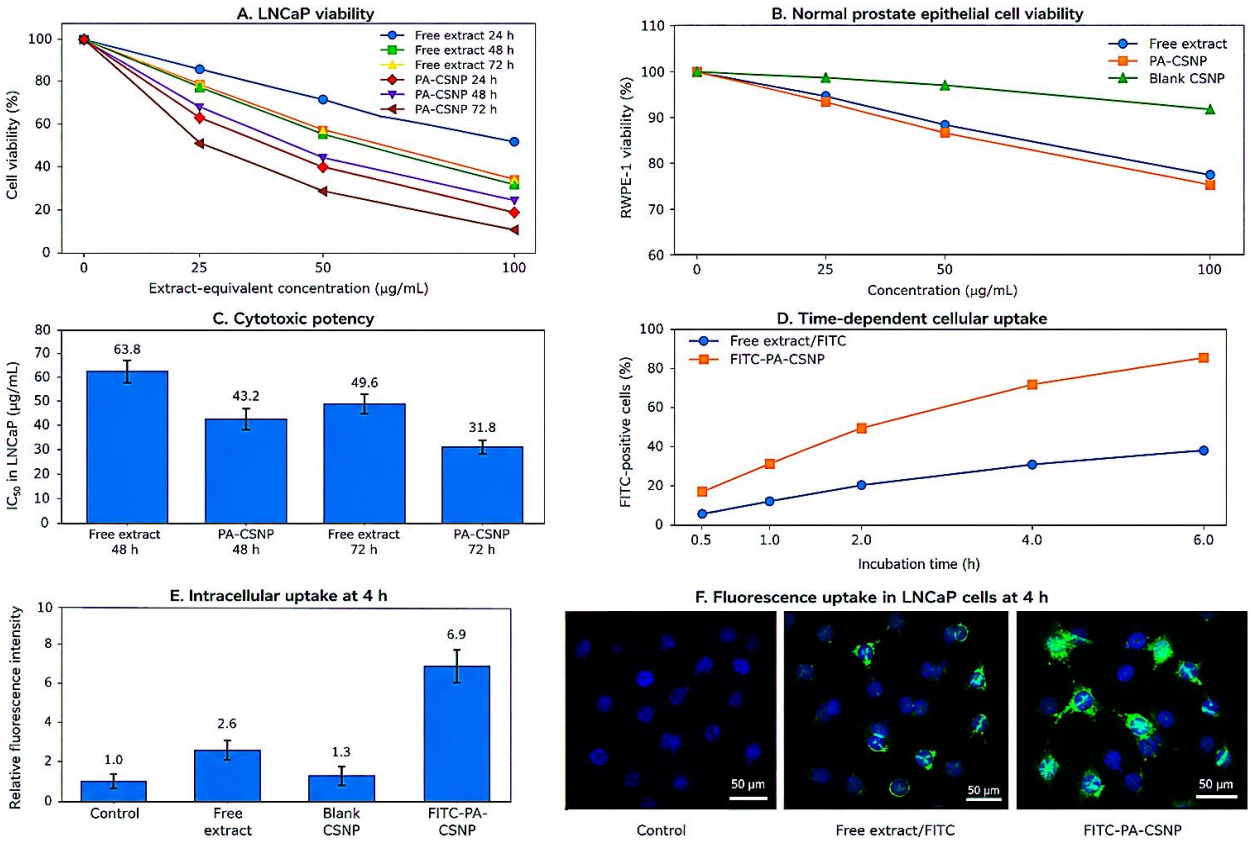

Figure 2: Viability and cellular uptake of *P. africana*-loaded chitosan nanoparticles in prostate cell models. **(A)** Dose- and time-dependent viability of LNCaP cells treated with free extract or nanoparticle-loaded extract at 25, 50, and 100 µg/mL for 24, 48, and 72 h**.** (B) Viability of RWPE-1 normal prostate epithelial cells treated with free extract, blank nanoparticles, or nanoparticle-loaded extract. (C) Comparative IC_{50} values at 48 and 72 h**.** (D) Time-dependent uptake of FITC-labelled nanoparticles over 0.5–6 h**.** (E) Relative fluorescence intensity at 4 h**.** (F) Fluorescence microscopy images showing enhanced intracellular nanoparticle uptake. Values are expressed as mean ± SD of triplicate determinations.

3.3.1. Selective index of *P. africana*-loaded CSNPs

Selectivity index analysis further demonstrated the preferential cytotoxicity of the formulations toward prostate cancer cells (Table 4). The *P. africana*-loaded chitosan nanoparticles exhibited higher selectivity than the free extract, with estimated SI values increasing from >2.31 at 48 h to >3.14 at 72 h. These findings indicate that nanoencapsulation enhanced not only the antiproliferative potency but also the selectivity of *P. africana* against LNCaP prostate cancer cells while minimizing toxicity toward normal RWPE-1 prostate epithelial cells.

Table 4: Cytotoxicity and selectivity index (SI) of *P. africana* formulations

Treatment	Time (h)	IC_{50} in LNCaP cells (µg/mL)	IC_{50} in RWPE-1 cells (µg/mL)	Selectivity index (SI)
Free *P. africana* extract	48	63.8	>100	>1.57
Free *P. africana* extract	72	49.6	>100	>2.02
P. africana-loaded CSNPs	48	43.2	>100	>2.31
P. africana-loaded CSNPs	72	31.8	>100	>3.14

SI = IC_{50} (RWPE-1 normal prostate epithelial cells) / IC_{50} (LNCaP prostate cancer cells). Because the IC_{50} value in RWPE-1 cells was not reached within the tested concentration range (0–100 µg/mL), SI values are expressed as minimum estimates. Higher SI values indicate greater selectivity toward prostate cancer cells relative to normal prostate epithelial cells.

3.4. Wound healing activity and transwell assay

The researchers examined the ability of *Prunus africana*-loaded chitosan nanoparticles to decrease TGF-β1-induced movement and invasion through three distinct assays, which included the wound-healing test, transwell migration assessment, and Matrigel invasion test. The results obtained from TGF-β1 treatment showed an increase in cell migration, which enabled improved wound closure

within 24 hours. The percentage wound closure increased from 46.2 ± 4.1% in the control group to 84.7 ± 5.2% in the TGF-β1-treated group (Figure 3A). The application of free *P. africana* extract decreased wound closure to 61.5 ± 4.8% while *P. africana*-loaded chitosan nanoparticles produced a stronger inhibitory effect, which reduced wound closure to 31.8 ± 3.6%. The SMAD3 inhibitor SIS3 group showed comparable results, which achieved 28.4 ± 3.1% wound closure.

The transwell migration results, which confirmed the wound-healing results, showed that TGF-β1 increased cell migration from 112 ± 10 cells/field in the control group to 242 ± 18 cells/field. Free *P. africana* extract reduced migration to 158 ± 13 cells/field, whereas *P. africana*-loaded chitosan nanoparticles further decreased migration to 84 ± 9 cells/field. The SIS3 treatment caused a similar effect, which resulted in 76 ± 8 migrated cells/field (Figure 3B). The Matrigel invasion assay showed that the nanoparticle formulation blocked invasive behavior, which demonstrated its anti-invasive properties. TGF-β1 increased the number of invaded cells from 94 ± 8 cells/field in the control group to 226 ± 17 cells/field. Free *P. africana* extract reduced invasion to 141 ± 11 cells/field, while *P. africana*-loaded chitosan nanoparticles suppressed invasion more effectively to 63 ± 7 cells/field. The SIS3 group showed 58 ± 6 invaded cells/field, supporting the involvement of SMAD3 signaling in TGF-β1-driven invasion (Figure 3C). *Prunus africana*-loaded chitosan nanoparticles significantly inhibited TGF-β1-induced cell migration by 64.8% and cell invasion by 69.2% relative to the TGF-β1-treated group ($p < 0.05$). The research outcomes show that *P. africana*-loaded chitosan nanoparticles block TGF-β1-induced cell movement and invasion, which produces effects that equal SMAD3 protein inhibition.

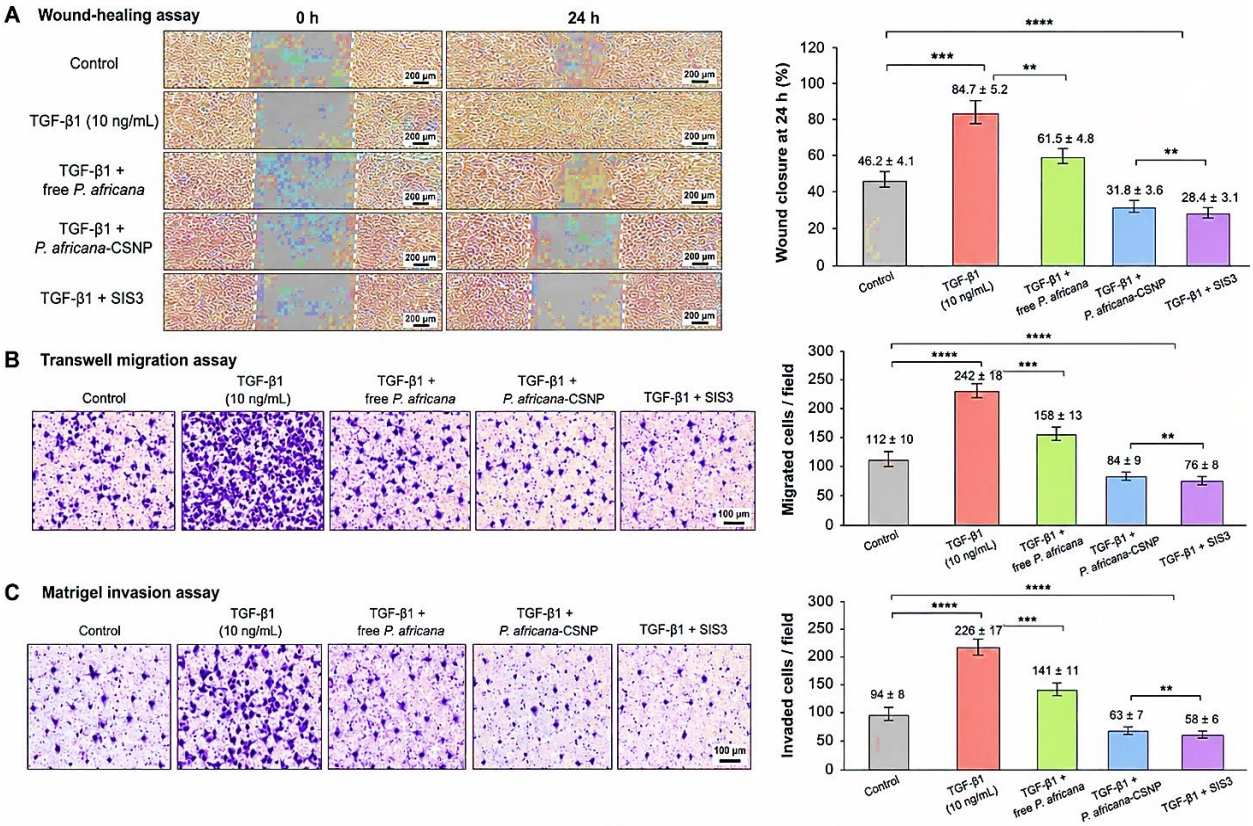

Figure 3: *Prunus africana*-loaded chitosan nanoparticles suppress TGF-β1-induced migration and invasion in LNCaP cells. (A) Representative wound-healing images at 0 h and 24 h, with quantification of wound closure. (B) Representative transwell migration images and migrated cell counts after 24 h**.** (C) Representative Matrigel invasion images and invaded cell counts after 48 h. TGF-β1 increased LNCaP cell migration and invasion, whereas free *P. africana* extract partially reduced these effects. *P. africana*-loaded chitosan nanoparticles showed stronger antimigratory and anti-invasive activity, comparable to SIS3. Data are presented as mean ± SD; n = 3. Values are statistical significance at *p<0.05, **p<0.01, ***p<0.001 vs control (one-way ANOVA followed by Tukey's post hoc test).

3.5. Expression of epithelial–mesenchymal transition (EMT) markers

Three methods were used to measure epithelial–mesenchymal transition markers: qRT-PCR, Western blotting, and immunofluorescence to study the effects of *Prunus africana*-loaded chitosan nanoparticles on TGF-β1-induced EMT reversal in LNCaP prostate cancer cells (Figure 4A-C). TGF-β1 treatment led to a significant decrease in CDH1 expression, from 1.00 in the control group to 0.38. The TGF-β1 treatment resulted in increased levels of CDH2, VIM, SNAI1, SNAI2, and TWIST1, which are proteins associated with mesenchymal and epithelial-mesenchymal transition, because their expression levels reached 2.84, 3.12, 2.66, 2.43, and 2.59 (Figure 4A). The *P. africana* extract showed partial restoration of these effects, whereas the *P. africana*-loaded

chitosan nanoparticles demonstrated stronger results by increasing CDH1 levels to 1.32 and decreasing CDH2, VIM, SNAI1, SNAI2, and TWIST1 values to 0.92, 1.08, 0.88, 0.84, and 0.89. The results produced effects that matched those of SIS3, which served as the SMAD3 inhibitor control.

Western blot analysis confirmed the transcriptional findings at the protein level (Figure 4B). TGF-β1 decreased E-cadherin protein levels while TGF-β1 increased N-cadherin, vimentin, and Snail, and phosphorylated SMAD3 levels, which demonstrated that TGF-β/SMAD3 signaling and epithelial-to-mesenchymal transition (EMT) were activated. Free *P. africana* extract treatment restored E-cadherin levels to some extent while it blocked the rise of mesenchymal protein levels. *P. africana*-loaded chitosan nanoparticles achieved better results because they brought E-cadherin levels back to normal, and they blocked vimentin and phosphorylated SMAD3 more effectively. The densitometric analysis showed that E-cadherin/GAPDH reached 1.26 in the nanoparticle-treated group, but it remained at 0.33 in the TGF-β1 group, while vimentin/GAPDH dropped from 2.08 to 0.38. The p-SMAD3/SMAD3 ratio decreased from 1.83 in the TGF-β1 group to 0.35 after nanoparticle treatment. The results were confirmed through immunofluorescence staining, which showed this condition in the test results (Figure 4C). Control cells displayed high E-cadherin staining, which attached to their membranes while showing low vimentin expression. The cells treated with TGF-β1 showed decreased E-cadherin levels while displaying strong vimentin staining, which showed that EMT had occurred. The free *P. africana* extract restored some epithelial characteristics, while the *P. africana*-loaded chitosan nanoparticles produced high E-cadherin staining results and low vimentin expression levels. The treatments produced effects that matched those found in the SIS3-treated group. The research findings show that *P. africana*-loaded chitosan nanoparticles successfully reversed TGF-β1-induced EMT through their ability to restore epithelial marker expression, their capacity to decrease mesenchymal marker levels, and their reduction of SMAD3 activation.

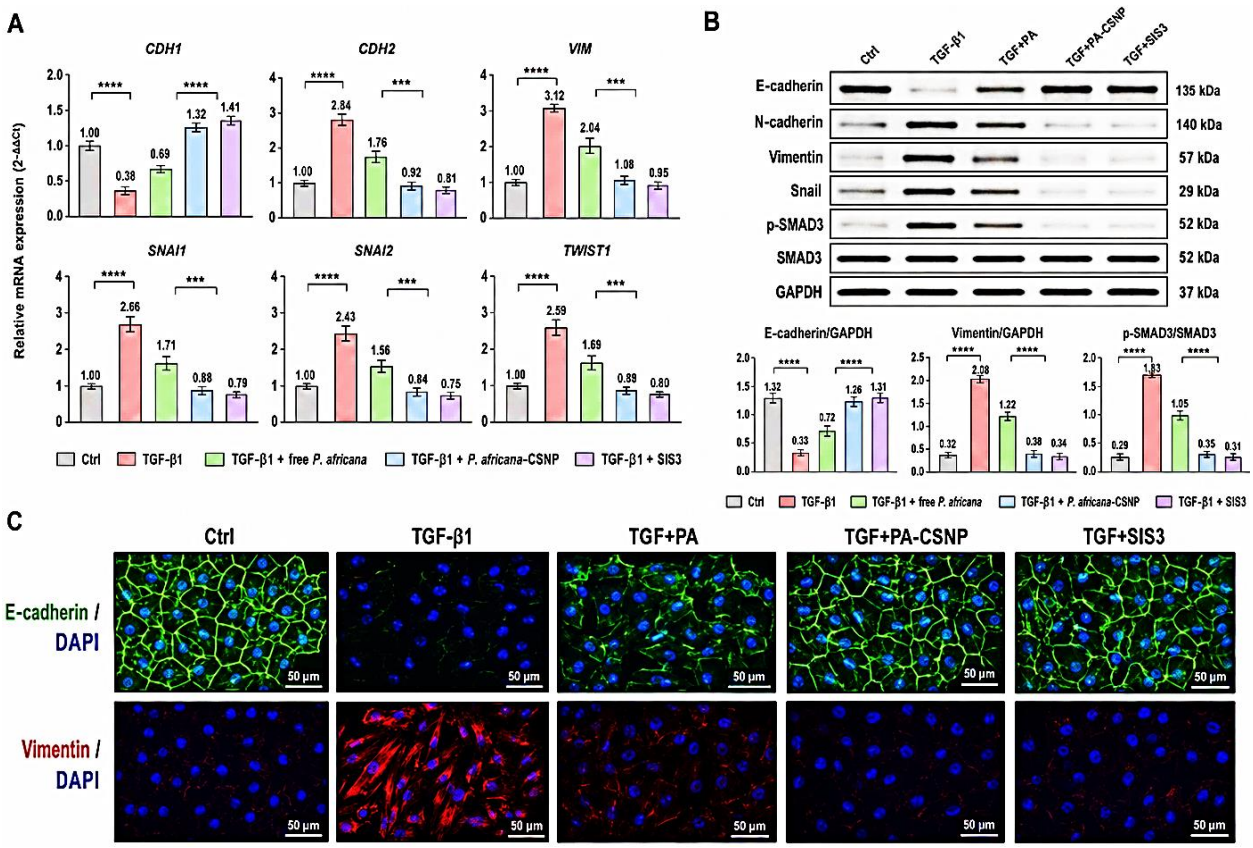

Figure 4: *P. africana*-loaded chitosan nanoparticles reverse TGF-β1-induced EMT marker dysregulation in LNCaP cells. (A) qRT-PCR analysis showing relative mRNA expression of CDH1, CDH2, VIM, SNAI1, SNAI2**,** and TWIST1 following treatment with TGF-β1, free *P. africana* extract, *P. africana*-loaded chitosan nanoparticles, or SIS3. (B) Western blot analysis and densitometric quantification of E-cadherin, N-cadherin, vimentin, Snail, p-SMAD3, SMAD3, and GAPDH. **(**C) Representative immunofluorescence images showing E-cadherin/DAPI and vimentin/DAPI staining across treatment groups. TGF-β1 induced EMT, whereas *P. africana*-loaded chitosan nanoparticles restored epithelial marker expression and suppressed mesenchymal marker expression, with effects comparable to SIS3. Data are presented as mean ± SD; n = 3. Values are statistical significance at *p<0.05, **p<0.01, ***p<0.001 vs control (one-way ANOVA followed by Tukey's post hoc test).

3.6. TGF-β/SMAD3 pathway activation

The study tested TGF-β/SMAD3 pathway activation to evaluate whether *P. africana* chitosan nanoparticles block epithelial-mesenchymal transition and invasion through TGF-β pathway inhibition (Figure 5A-C). The TGF-β1 treatment resulted in higher mRNA levels of TGFB1, SMAD3, MMP2, and MMP9, which showed that the signaling pathways for epithelial-mesenchymal transition and invasion were now active. The free *P. africana* extract reduced gene expression levels, but the *P. africana*-loaded chitosan nanoparticles achieved more effective

suppression, which brought most transcript levels back to their control values. The effect matched the level of the SMAD3 inhibitor SIS3 (Figure 5A). Western blot analysis confirmed that the proteins showed pathway modulation according to the results shown in Figure 5B. TGF-β1 treatment led to increased levels of TGF-β1 and phosphorylated SMAD3 and phosphorylated SMAD2 protein, while total SMAD3 levels stayed almost the same. The P. africana-loaded chitosan nanoparticles treatment resulted in a significant decrease of TGF-β1 and p-SMAD3 and p-SMAD2 levels when compared to TGF-β1 treatment and the free extract treatment. TGF-β1-treated cells displayed strong nuclear p-SMAD3 localization, but nanoparticle treatment reduced the number of cells that showed nuclear p-SMAD3-positive results (Figure 5C; SM 1). The research demonstrates that *P. africana*-loaded chitosan nanoparticles block TGF-β/SMAD3 pathway activation, which leads to downstream invasion-related mediators in LNCaP cells.

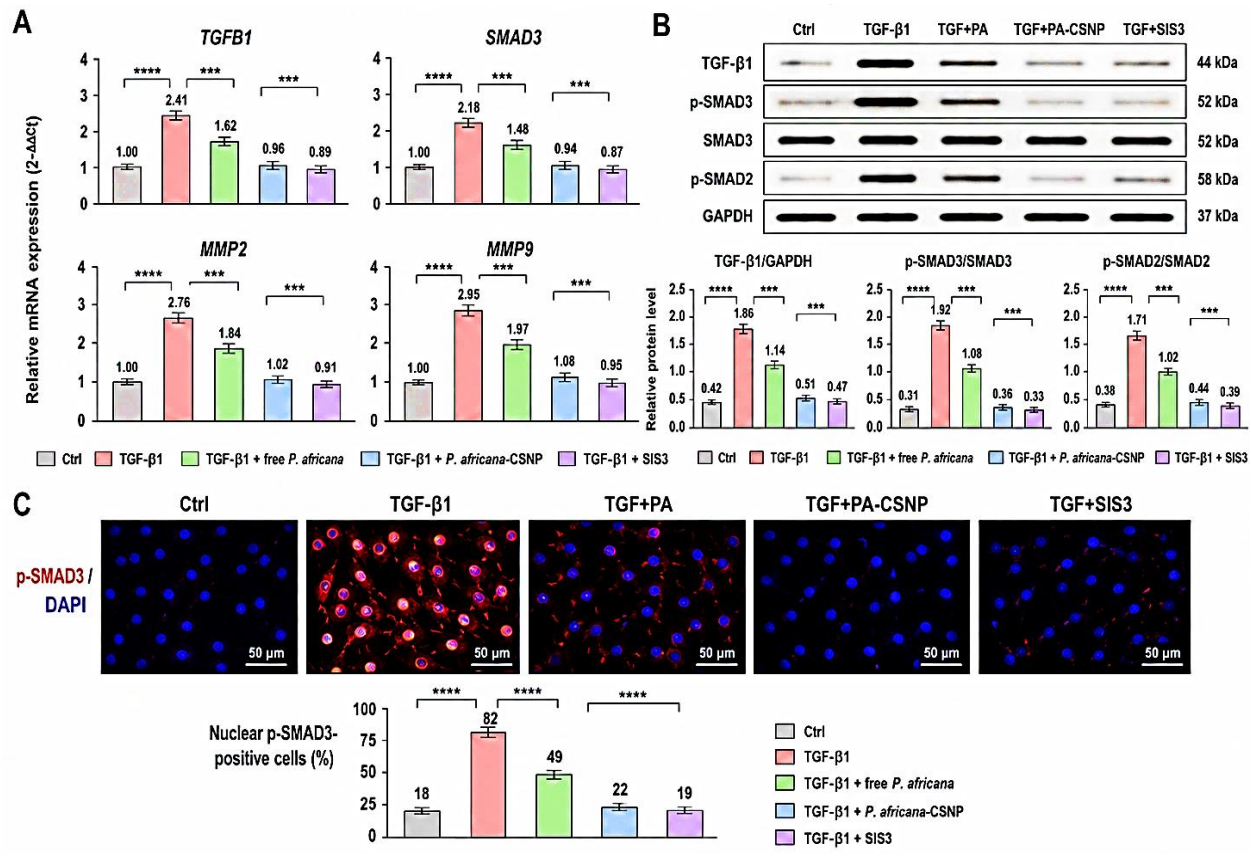

Figure 5: *Prunus africana*-loaded chitosan nanoparticles suppress TGF-β/SMAD3 signaling in LNCaP cells. (A) qRT-PCR analysis of TGFB1, SMAD3, MMP2**,** and MMP9 expression following treatment with TGF-β1, free *P. africana*, *P. africana*-loaded chitosan nanoparticles, or SIS3. (B) Western blot analysis and densitometric quantification of TGF-β1, p-SMAD3, SMAD3, p-SMAD2, and GAPDH. (C) Immunofluorescence images and quantification of nuclear p-SMAD3-positive cells. TGF-β1 activated

canonical SMAD signaling, whereas *P. africana*-loaded chitosan nanoparticles suppressed SMAD pathway activation and invasion-associated mediators, with effects comparable to SIS3. Data are presented as mean ± SD**;** n = 3**.** Values are statistical significance at *p<0.05, **p<0.01, and ###p<0.001 vs control (one-way ANOVA followed by Tukey's post hoc test).

3.7. *In vivo* anti-metastasis effects

The study evaluated the antimetastatic properties of *Prunus africana*-loaded chitosan nanoparticles using three assessment methods: evaluating metastatic burden, examining tissue histology, and analyzing epithelial–mesenchymal transition (EMT) and EMT-related immunohistochemical markers. The study results in Figure 6A demonstrate that TGF-β1 treatment led to higher numbers of metastatic lung and liver nodules than in the control group. The free *P. africana* extract treatment decreased metastatic nodules, but the *P. africana*-loaded chitosan nanoparticles treatment produced a more effective decrease of lung and liver metastases. The nanoparticle formulation showed similar results to the SMAD3 inhibitor SIS3. Histological examination by H&E staining confirmed extensive metastatic infiltration in the TGF-β1 group, particularly in the lung and liver tissues (Figure 6B). The animals treated with *P. africana*-loaded chitosan nanoparticles demonstrated an improvement in their condition because they developed smaller and fewer metastatic tumors, which maintained their original tissue structure. The TGF-β1 treatment caused E-cadherin level decrease while it elevated N-cadherin, vimentin, and Ki-67, and MMP-9 levels within metastatic regions according to immunohistochemical analysis (Figure 6C–D; SM 2). The nanoparticle treatment restored E-cadherin staining while it substantially reduced the presence of mesenchymal, proliferative, and invasion-related indicators. As shown in Figure 6D, TGF-β1 stimulation significantly enhanced the migratory and invasive capacities of LNCaP cells compared with untreated controls. Treatment with PA-CSNP markedly suppressed these metastatic phenotypes. Quantitative analysis revealed that PA-CSNP inhibited TGF-β1-induced cell migration by 64.8% and cell invasion by 69.2% relative to the TGF-β1-treated group ($p < 0.001$). Animals treated with PA-CSNP exhibited a substantial reduction in the number of metastatic lung nodules compared with the untreated metastatic control group (Figure 6E). Specifically, PA-CSNP treatment reduced lung metastasis burden by 58.7% ($p < 0.01$), demonstrating significant inhibition of tumor dissemination and colonization in distant organs. These findings indicate that PA-CSNP effectively suppresses key steps involved in cancer metastasis, including cellular migration, invasion, and secondary tumor formation.

The schematic summary in Figure 6E shows that *P. africana*-loaded chitosan nanoparticles weakened TGF-β/SMAD-based EMT transmission, which led to lower levels of migration, invasion, and metastatic spread.

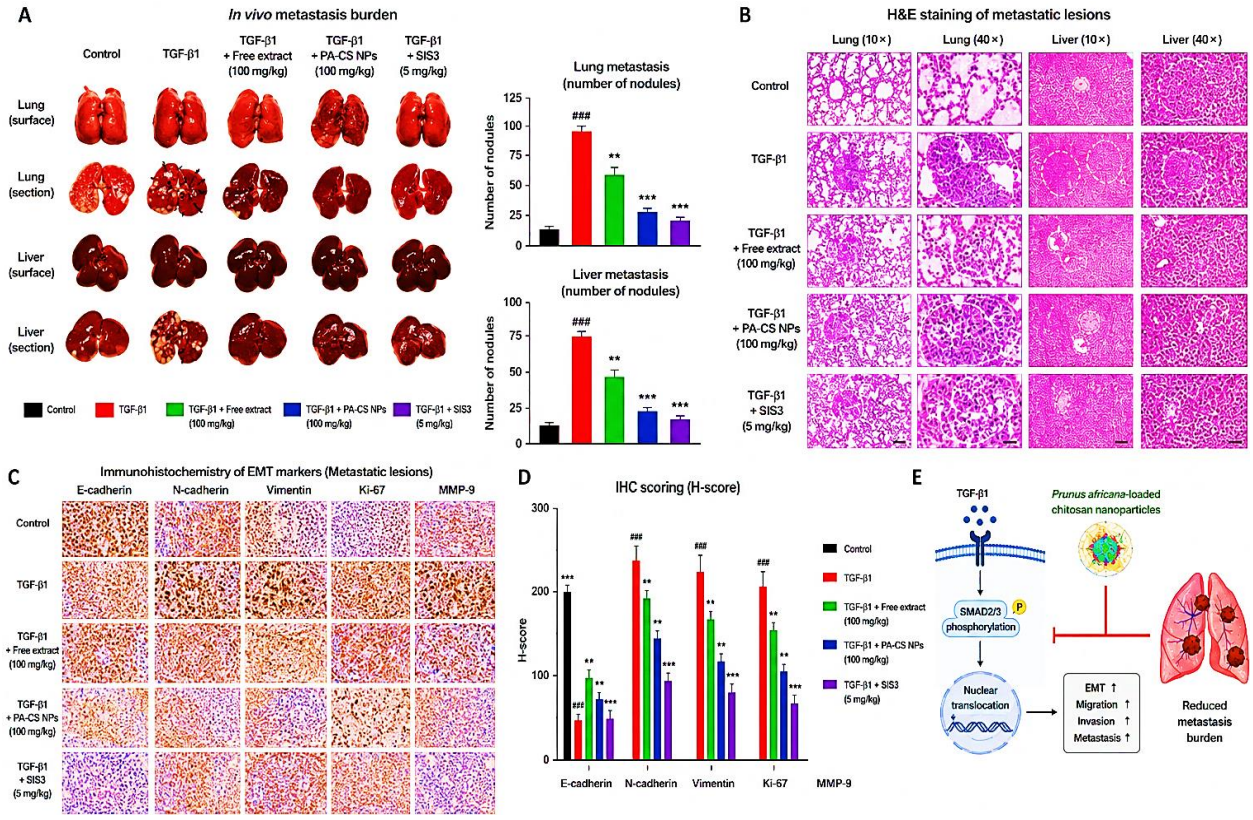

Figure 6: *P. africana*-loaded chitosan nanoparticles suppress in vivo metastasis and EMT-associated marker expression. (A) Lung and liver images with quantification of metastatic nodules across treatment groups. (B) H&E-stained lung and liver sections showing metastatic lesion distribution. (C) Immunohistochemical staining of E-cadherin, N-cadherin, vimentin, Ki-67, and MMP-9 in metastatic lesions. (D) Quantitative H-score analysis of EMT, proliferation, and invasion markers. (E) Proposed mechanism showing inhibition of TGF-β/SMAD signaling by *P. africana*-loaded chitosan nanoparticles, leading to reduced EMT, migration, invasion, and metastasis. Data are presented as mean ± SD**;** n = 6 animals per group. Values are statistical significance at *p<0.05, **p<0.01, and ###p<0.001 vs control (one-way ANOVA followed by Tukey's post hoc test).

4. Discussion

This study provides preclinical evidence that chitosan nanoparticle delivery may enhance the antimetastatic activity of *Prunus africana* against prostate cancer by suppressing TGF-β/SMAD3-driven epithelial–mesenchymal transition. Compared to the free extract, the prepared nanoparticles showed better physicochemical properties, enhanced cellular absorption, prolonged release, and

higher biological activity. These results lend credence to the more general idea that plant-derived anticancer drugs, whose therapeutic efficacy could ordinarily be constrained by poor solubility, instability, or insufficient intracellular accumulation, can be delivered via nanocarriers [32].

Because the epithelial–mesenchymal transition is a major factor in the spread of prostate cancer, the antimetastatic effect seen in this study is mechanistically significant. Prostate cancer cells developed a mesenchymal phenotype in the TGF-β-induced model, characterized by decreased E-cadherin and increased N-cadherin, vimentin, Snail, Slug, Twist, and matrix metalloproteinases. These alterations align with the known function of TGF-β signaling in advanced cancer metastatic development, invasion, immune evasion, and epithelial plasticity [8,37,38]. The ability of *P. africana*-loaded chitosan nanoparticles to reverse these alterations suggests that the formulation does not merely suppress cell viability but also interferes with metastatic signaling programs.

SMAD3 appears to be a key molecular target of the observed response. In advanced prostate cancer, activation of TGF-β signaling may shift from tumor suppression to tumor promotion, partly through SMAD-dependent transcriptional induction of epithelial–mesenchymal transition regulators[10, 39]. In this study, nanoparticle treatment reduced TGF-β-induced SMAD3 phosphorylation and nuclear localization, accompanied by downregulation of epithelial–mesenchymal transition (EMT) transcription factors. This suggests that *P. africana* bioactives may suppress EMT by interfering with canonical TGF-β/SMAD3 signaling. However, because TGF-β also activates non-SMAD pathways, including PI3K/AKT, MAPK, RhoA, and mTOR [10]. Additional pathway-level studies are needed to determine whether these mechanisms also contribute to the observed phenotype.

The combined effects of *P. africana's* phytochemical components may be reflected in its biological activity. Prior research has connected *P. africana* extracts and components to growth-inhibitory, pro-apoptotic, antiandrogenic, and antiangiogenic actions in models of prostate cancer. By presenting *P. africana* as a possible regulator of EMT-associated metastatic signaling, the current draft's suggested mechanism expands this pharmacological profile. Crucially, multi-targeted action may be possible with the use of whole or standardized extract; however, this also presents issues with phytochemical variability, quality control, reproducibility, and regulatory standards.

Because of its cationic nature, mucoadhesive qualities, biodegradability, biocompatibility, and aptitude for ionic gelation, chitosan was chosen as a nanocarrier [17]. Improved uptake may result from a positive nanoparticle surface's ability to interact with negatively charged cell membranes. The intracellular exposure to *P. africana* bioactives may be further maintained by sustained release. The observed antimetastatic effect may have been facilitated by better distribution, as evidenced by the higher activity of the nanoparticle-loaded extract when compared to the free extract. There are restrictions on the study. First, because *P. africana* extract is chemically complex, more research is needed to identify the precise components that decrease SMAD3. Second, the intricacy of tumor microenvironment interactions, stromal signaling, immunological regulation, and metastatic niche creation cannot be accurately replicated by *in vitro* EMT models. Third, whereas in vivo metastatic models enhance translational value, they might not accurately represent the course of clinical prostate cancer. Fourth, before clinical translation, long-term toxicity, pharmacokinetics, biodistribution, immunogenicity, and reproductive safety should be assessed.

While our findings demonstrate that *Prunus africana*-loaded chitosan nanoparticles effectively suppress TGF-β/SMAD3 signaling and invasion-associated mediators in LNCaP cells, the study has certain limitations. First, although preliminary assays indicated that blank chitosan nanoparticles did not alter SMAD pathway activation, we did not include a formal free extract + blank nanoparticle combination group in the main experiments, which would further exclude potential carrier-related effects. Second, our mechanistic validation relied on pharmacological inhibition of SMAD3 (SIS3), and we did not perform complementary SMAD3 overexpression or recovery experiments. Such gain-of-function approaches would provide additional confirmation that SMAD3 is the central target of *P. africana*. These aspects represent important directions for future work to strengthen the mechanistic understanding of *P. africana*-mediated suppression of TGF-β signaling. Bioactivity-guided fractionation, metabolomic profiling, pharmacokinetic analysis, nanoparticle biodistribution, orthotopic and bone-metastasis models, and combination studies with TGF-β pathway inhibitors, docetaxel, or androgen receptor inhibitors should all be included in future research. Testing of *P. africana*-loaded nanoparticles that inhibit cancer stemness, circulating tumor cell survival, anoikis resistance, and bone colonization would also be beneficial.

5. Conclusions

By enhancing cellular absorption, maintaining phytochemical release, inhibiting migration and invasion, and reducing TGF-β/SMAD3-driven epithelial–mesenchymal transition, chitosan nanoparticle delivery improved *Prunus africana's* antimetastatic effectiveness in prostate cancer models. *In vivo* metastatic burden was decreased, mesenchymal and invasion-associated indicators were diminished, and epithelial marker expression was restored by the formulation. The development of *P. africana*-loaded chitosan nanoparticles as a promising nanophytotherapeutic platform for reducing prostate cancer metastasis is supported by our findings. In clinically relevant metastatic prostate cancer models, additional research should establish safety, optimize pharmacokinetics, validate the active ingredients, and assess therapeutic efficacy.

List of Abbreviations

EMT	Epithelial–mesenchymal transition
TGF-β	Transforming growth factor-beta
SMAD3	Mothers against decapentaplegic homolog 3
TPP	Sodium tripolyphosphate
PDI	Polydispersity index
qRT-PCR	Quantitative real-time polymerase chain reaction
MMP	Matrix metalloproteinase
PBS	Phosphate-buffered saline
CSNP	Chitosan Nanoparticles

LNCaP	Lymph Node Carcinoma of the Prostate
FITC	Fluorescein Isothiocyanate
DAPI	4',6-diamidino-2-phenylindole
H&E	Hematoxylin and Eosin
CDH1	Cadherin 1 (E-cadherin)
CDH2	Cadherin 2 (N-cadherin)
VIM	Vimentin

Author Contributions

Conceptualization, writing- original draft preparation, methodology, validation, formal analysis, investigation, supervision, writing- review and editing: **C.A.U.;** Resources, writing- review and editing, investigation, visualization, project administration, methodology: **H.B.Y**. All authors have read and agreed to the published version of the manuscript.

Availability of Data and Originality

The datasets generated and analyzed during the present study are original data and are included in the manuscript and supplementary material.

Ethical Commetti Approval and Consent to Participate:

All animal experiments were reviewed and approved by the Animal Research and Ethical Committee, Department of Pharmacology and Toxicology, Faculty of Pharmacy, University of Maiduguri, under protocol number FP/03/24/SP.9788, approved on March, 2025. Human-derived prostate cancer (LNCaP) and normal prostate epithelial (RWPE-1) cell lines used in this study were obtained from the American Type Culture Collection (ATCC, Manassas, VA, USA). The study did not involve the recruitment of human participants, the collection of human tissues, or the use of identifiable human data. Therefore, informed consent was not required. The experiments were conducted exclusively using commercially available established cell lines. Where applicable, all institutional requirements governing the use of commercially acquired human cell lines were followed.

Animals Rights:

All animal procedures were conducted in accordance with internationally accepted guidelines for the care and use of laboratory animals and complied with the principles of the Basel Declaration. Furthermore, the study was designed, conducted, and reported in accordance with the ARRIVE

(Animal Research: Reporting of *In Vivo* Experiments) Guidelines to ensure transparency, reproducibility, and responsible animal research practices.

Consent for Publication

Not applicable.

Conflicts of Interest

The authors declare no conflicts of interest.

Funding

No external funding was received for this research.

Acknowledgments

The authors acknowledged Mr. Yusuf Babagana for his technical assistance during this work.

AI Declaration

The authors acknowledged the use of Grammarly and Autopilot to improve grammar and readability during manuscript preparation. The authors take full responsibility of manuscript content.

Supplementary Material:

Supplementary material associated with this article has been published online and is available at: Link to the DOI

References

[1] Amanda, E.U.; Josephine, E.O.O.; Innocent, I.O. Effect of *Annona muricata* Leaf Ethanol Extract on Testosterone-Induced Benign Prostatic Hyperplasia in Wistar Rats. *Biosci. J.* **2024**, 12, 12–23.

[2] Thomas-Charles, C.; Fennell, H. Anti-Prostate Cancer Activity of Plant-Derived Bioactive Compounds: A Review. *Curr. Mol. Biol. Rep.* **2019**, 5, 140–151.

[3] Wasim, S.; Lee, S.Y.; Kim, J. Complexities of Prostate Cancer. Int. J. Mol. Sci. **2022**, 23, 14257. doi:10.3390/ijms232214257.

[4] Nelson, V.K.; Sahoo, N.K.; Sahu, M.; Sudhan, H.H.; Pullaiah, C.P.; Muralikrishna, K.S. *In Vitro* Anticancer Activity of *Eclipta alba* Whole Plant Extract on Colon Cancer Cell HCT-116. *BMC Complement. Med. Ther.* **2020**, 20, 1–8.

[5] Krock, B.L.; Skuli, N.; Simon, M.C. Hypoxia-Induced Angiogenesis: Good and Evil. *Genes Cancer* **2011**, 2, 1117–1133.

[6] Yang, C.; Li, Y.; Fu, L.; Jiang, T.; Meng, F. Betulinic Acid Induces Apoptosis and Inhibits Metastasis of Human Renal Carcinoma Cells *In Vitro* and *In Vivo*. *J. Cell. Biochem.* **2018**, 119, 8611–8622.

[7] Wicks, E.E.; Semenza, G.L. Hypoxia-Inducible Factors: Cancer Progression and Clinical Translation. *J. Clin. Investig.* **2022**, 132, 1–10.

[8] Suzuki, K., Fujimoto, N., Shiota, M. *et al.* Recent advances in drug treatment for prostate cancer. *Jpn J Radiol*. **2025**,43, 1618–1627.doi:10.1007/s11604-025-01816-3.

[9] Zeng, M.; Zhu, L.; Li, L.; Kang, C. miR-378 Suppresses the Proliferation, Migration and Invasion of Colon Cancer Cells by Inhibiting SDAD1. *Cell. Mol. Biol. Lett.* **2017**, 22, 1–13.

[10] Jia, L.; Jin, H.; Zhou, J.; Chen, L.; Lu, Y.; Ming, Y.; et al. A Potential Anti-Tumor Herbal Medicine, Corilagin, Inhibits Ovarian Cancer Cell Growth through Blocking the TGF-β Signaling Pathways. *BMC Complement. Altern. Med.* **2013**, 13, 33. doi:10.1186/1472-6882-13-33

[11] Li, L.; He, L.; Wu, Y.; Zhang, Y. Carvacrol Affects Breast Cancer Cells through TRPM7-Mediated Cell Cycle Regulation. *Life Sci.* **2021**, 266, 118894.

[12] Sharma, M.; Kashyap, N.; Verma, M.; Devi, B.; Prashar, A.; Sinha, S. Role of Natural Products in Cancer Management: A Comprehensive Review. *J. Ethnopharmacol. Toxicol.* **2024**, 2, 1–18.

[13] Rincón, P.Q.; Gallardo, K.C.; Verbel, J.O. Natural Anticancer Agents: Prospection of Medicinal and Aromatic Plants in Modern Chemoprevention and Chemotherapy. *Nat. Prod. Bioprospect.* **2025**.

[14] Asuzu, P.; Aryee, A.; Trompeter, N.; Mann, Y.; Besong, S.; Duncan, R.; et al. *In Vitro* Assessment of Efficacy and Cytotoxicity of *Prunus africana* Extracts on Prostate Cancer C4-2 Cells. *bioRxiv* **2021**, 1–24.

[15] Komakech, R.; Yim, N.H.; Shim, K.S.; Jung, H.; Byun, J.E.; Lee, J.; et al. Root Extract of a Micropropagated *Prunus africana* Medicinal Plant Induced Apoptosis in Human Prostate Cancer Cells (PC-3) via Caspase-3 Activation. *Evid.-Based Complement. Altern. Med.* **2022**, 2022.

[16] Raj, V.; Mishra, A.K.; Mishra, A.; Khan, N.A. Hepatoprotective Effect of *Prunus armeniaca* L. (Apricot) Leaf Extracts on Paracetamol-Induced Liver Damage in Wistar Rats. *Pharmacogn. J.* **2016**, 8, 154–158.

[17] Sultan, M.H.; Moni, S.S.; Madkhali, O.A.; Bakkari, M.A.; Alshahrani, S.; Alqahtani, S.S.; et al. Characterization of Cisplatin-Loaded Chitosan Nanoparticles and Rituximab-Linked Surfaces as Target-Specific Injectable Nano-Formulations for Combating Cancer. *Sci. Rep.* **2022**, 12, 1–16.

[18] Ukwubile, C.A. *Lantana camara* L. Leaf Extract-Loaded Chitosan Nanoparticles Induce Apoptosis and Suppress PI3K/AKT and NF-κB Signaling in Triple-Negative Breast (MDA-MB-231) and Colorectal Cancer (HCT116) Cells. **2025**, 22, 185–194.

[19] Kumar, D.A.; Dharmendra, S.; Jhansee, M.; Shrikant, N.; P., P.S.; S., V.B. Development and Characterization of Chitosan Nanoparticles. *Int. Res. J. Pharm.* **2011**, 2, 145–151.

[20] Ngouana, V.; Ngoumou, J.M.; Kamdem, B.P.; Youbi, A.K.; Makemteu, J.; Nangap, M.J.T.; et al. Phytochemical Screening, Antiplasmodial and Antioxidant Activities of *Combretum rhodanthum* Extracts. *South Asian J. Parasitol.* **2025**, 8, 66–81.

[21] Salehi, B.; Fokou, P.V.T.; Yamthe, L.R.T.; Tali, B.T.; Adetunji, C.O.; Rahavian, A.; et al. Phytochemicals in Prostate Cancer: From Bioactive Molecules to Upcoming Therapeutic Agents. *Nutrients* **2019**, 11, 1–42.

[22] Anes Ukwubile, C.; Nuhu, A.; Clement Famurewa, A.; Nettey, H.; Amakaeze Odugu, J. Chitosan Nanoparticles Encapsulating *Ipomoea digitata* L. Tuber and *Jatropha gossypiifolia* L. Leaf Extract Suppress NF-κB, Wnt/β-Catenin, and MAPK Signaling Pathways in HCT116 and SW480 Colorectal Cancer Cells. *Int. J. Adv. Multidiscip. Res. Stud.* **2025**, 5, 45–58.

[23] Basehore, S.E.; Garcia, J.; Clyne, A.M. Steady Laminar Flow Decreases Endothelial Glycolytic Flux While Enhancing Proteoglycan Synthesis and Antioxidant Pathways. **2024**.

[24] Foster, K.; Oyenihi, O.; Rademan, S.; Erhabor, J.; Matsabisa, M.; Barker, J.; et al. Selective Cytotoxic and Anti-Metastatic Activity in DU-145 Prostate Cancer Cells Induced by *Annona muricata* L. Bark Extract and Phytochemical, Annonacin. *BMC Complement. Med. Ther.* **2020**, 20, 1–15.

[25] Wei, W.; Guo, Q.; Guo, C.; Cui, X.; Ma, X.; Shen, X.; et al. Ginsenoside Rh2 Suppresses Metastasis and Growth of Colon Cancer via miR-491. *J. Oncol.* **2021**, 2021.

[26] Ukwubile, C.A.; Lawan, M.Z.; Malgwi, T.S.; Yesufu, H.B. Evaluation of Anti-Inflammatory and Anticancer Activities of *Maerua angolensis* DC. Leaf Extract-Loaded Chitosan Nanoparticles. *Biomater. Connect.* **2025**, 1–15.

[27] Hanna, D.H.; Al-Atmani, A.K.; AlRashidi, A.A.; Shafee, E.E. *Camellia sinensis* Methanolic Leaves Extract: Phytochemical Analysis and Anticancer Activity against Human Liver Cancer Cells. *PLoS ONE* **2024**, 19, e0309795.

[28] Pal, A.; Sanyal, S.; Das, S.; Sengupta, T.K. Effect of *Lantana camara* Ethanolic Leaf Extract on Survival and Migration of MDA-MB-231 Triple-Negative Breast Cancer Cell Line. *J. Herb. Med.* **2024**, 43, 100837.

[29] Guo, J.; Liu, Y. INHBA Promotes the Proliferation, Migration and Invasion of Colon Cancer Cells through the Upregulation of VCAN. *J. Int. Med. Res.* **2021**, 49.

[30] Justus, C.R.; Leffler, N.; Ruiz-Echevarria, M.; Yang, L.V. *In Vitro* Cell Migration and Invasion Assays. *J. Vis. Exp.* **2014**, 88.

[31] Zhu, T.; Liu, T.J.; Shi, Y.Y.; Zhao, Q. Vitamin D/VDR Signaling Pathway Ameliorates 2,4,6-Trinitrobenzene Sulfonic Acid-Induced Colitis by Inhibiting Intestinal Epithelial Apoptosis. *Int. J. Mol. Med.* **2015**, 35, 1213–1218.

[32] da Silva, W.N.; Carvalho Costa, P.A.; Scalzo Júnior, S.R.A.; Ferreira, H.A.S.; Prazeres, P.H.D.M.; Campos, C.L.V.; et al. Ionizable Lipid Nanoparticle-Mediated TRAIL mRNA Delivery in the Tumor Microenvironment to Inhibit Colon Cancer Progression. *Int. J. Nanomed.* **2024**, 19, 2655–2673.

[33] Buccato, D.G.; Ullah, H.; De Lellis, L.F.; Piccinocchi, R.; Baldi, A.; Xiao, X.; et al. *In Vitro* Assessment of Cortisol Release Inhibition, Bioaccessibility and Bioavailability of a Chemically Characterized *Scutellaria lateriflora* L. Hydroethanolic Extract. *Molecules* **2024**, 29.

[34] Zhang, X.; Xu, R.; Feng, W.; Xu, J.; Liang, Y.; Mu, J. Autophagy-Related Genes Contribute to Malignant Progression and Have a Clinical Prognostic Impact in Colon Adenocarcinoma. *Exp. Ther. Med.* **2021**, 22, 1–11.

[35] Jamieson, S.; Butzow, R.; Andersson, N.; Alexiadis, M.; Unkila-Kallio, L.; Heikinheimo, M.; et al. The FOXL2 C134W Mutation Is Characteristic of Adult Granulosa Cell Tumors of the Ovary. *Mod. Pathol.* **2010**, 23, 1477–1485.

[36] Liu, X.P.; Zhou, S.T.; Li, X.Y.; Chen, X.C.; Zhao, X.; Qian, Z.Y.; et al. Anti-Tumor Activity of N-Trimethyl Chitosan-Encapsulated Camptothecin in a Mouse Melanoma Model. *J. Exp. Clin. Cancer Res.* **2010**, 29, 1–9.

[37] Nie, D.; Fu, J.; Chen, H.; Cheng, J.; Fu, J. Roles of MicroRNA-34a in Epithelial to Mesenchymal Transition, Competing Endogenous RNA Sponging and Its Therapeutic Potential. *Int. J. Mol. Sci.* **2019**, 20.

[38] Jayachandran, P.; Battaglin, F.; Strelez, C.; Lenz, A.; Algaze, S.; Soni, S.; et al. Breast Cancer and Neurotransmitters: Emerging Insights on Mechanisms and Therapeutic Directions. *Oncogene* **2023**, 42, 627–637.

[39] Zhao, H.; Wu, L.; Yan, G.; Chen, Y.; Zhou, M.; Wu,Y.; et al. Inflammation and Tumor Progression: Signaling Pathways and Targeted Intervention. *Signal Transduct. Target. Ther.* **2021**, 6.